EARTHQUAKE ENGINEERING AND STRUCTURAL DYNAMICS
Earthquake Engng. Struct. Dyn. **27**, 577–588 (1998)

OPTIMUM STRENGTH RATIO OF HYSTERETIC DAMPER

KAZUO INOUE† AND SUSUMU KUWAHARA*‡
Architectural Engineering, Faculty of Engineering, Osaka University, Yamadaoka 2-1, Suita City, Osaka 565, Japan

SUMMARY

This paper deals with steel moment frames combined with hysteretic dampers. Specifically, it examines the strength of dampers required to minimize damage to moment frames under earthquake loading. The important structural variables are the ratio of the dampers' shear strength to the maximum resistance, termed β in this study, and the relative stiffness between the damper and the main frame, termed k. The equivalent viscous damping ratio of the entire structural system is affected by the quantities β and k and the ductility ratio of the main frame. The optimum dampers' strength ratio (β_{opt}), which maximizes the equivalent viscous damping ratio, was formulated as a function of k, and it was found that β_{opt} is independent of the ductility ratio of the main frame. Earthquake response analysis confirmed that damage to the main frame can be significantly reduced by hysteretic dampers and minimized at the value of β_{opt}.

KEY WORDS: hysteretic damper; equivalent viscous damping ratio; optimum damper's strength ratio; earthquake response

INTRODUCTION

In recent years, research has been flourishing on the development of various damping mechanisms intended to provide positive control of structural vibration induced by earthquakes. Details of these damping mechanisms and their applications have been reported in numerous publications (References[1–3] among many others). These damping mechanisms include viscous dampers, viscoelastic dampers, hysteretic dampers and others. Hysteretic dampers dissipate the energy exerted into the structure by their hysteresis; Figure 1 shows three types of hysteretic dampers incorporated into building frames. The ADAS device,[4,5] the TADAS device,[6] and the steel shear panel[7,8] are examples of the elastoplastic element shown in Figure 1(a). The friction damper[9–11] shown in Figure 1(b) dissipates seismic energy by mechanical slipping. One example of such a device is the thermally sprayed aluminium friction damper,[11] whose hysteresis is as shown in Fig. 2. The buckling-restrained steel brace shown in Figure 1(c) is a steel brace stiffened by a steel tube to prevent buckling of the steel brace when subjected to compression. Hysteretic curves of such a buckling-restrained H-shaped steel brace are shown in Figure 3.[12] Both the elastoplastic element and the buckling-restrained steel brace exhibit elastic–plastic hysteretic behaviour, whereas the hysteretic behaviour of friction dampers is rigid-plastic, as shown in Figure 3. However, the supporting members are not rigid [Figure 1(b)], so that the friction damping system as a whole behaves elastoplastically.

It is known that the energy input during an earthquake is relatively independent of the restoring force characteristics of the structural system.[13–17] This fact suggests that damage to the main frame can be reduced effectively by adequately incorporating hysteretic dampers into the structure. Here, selection of the strength

* Correspondence to: Susumu Kawahara, Department of Architectural Engineering, Faculty of Engineering, Osaka University, Yamadaoka 2-1, Suita City, Osaka 565, Japan. E-mail: kuwa@arch.eng.osaka-u.ac.jp
† Associate Professor
‡ Assistant Professor

CCC 0098–8847/98/060577–12$17·50

Received 30 October 1996
Revised 17 April 1997 and 30 October 1997

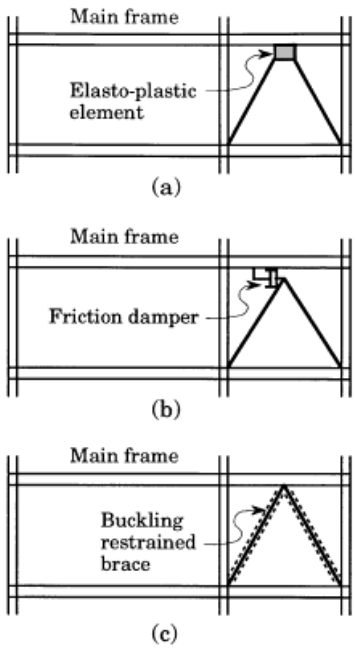

Figure 1. Examples of hysteretic dampers incorporated into building frames

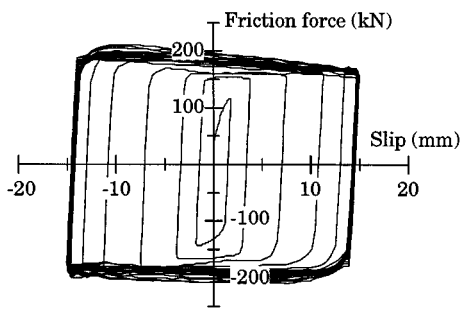

Figure 2. Hysteresis of a thermally sprayed aluminium friction damper (Reference 3)

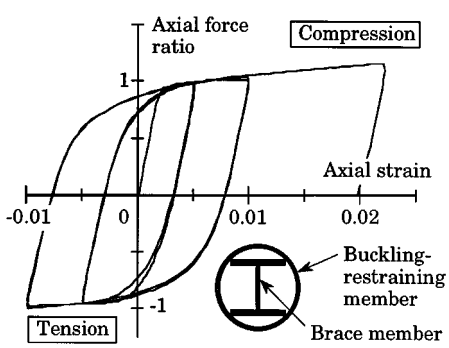

Figure 3. Cyclic axial force vs. axial strain relation of a buckling-restrained steel brace (Reference 2)

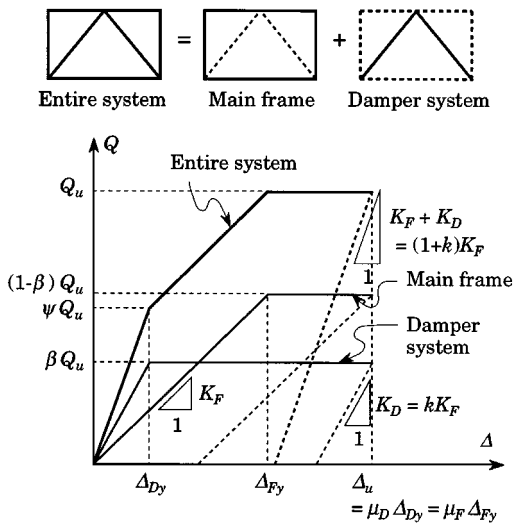

Figure 4. Schematic hysteretic behaviour of a structure with a hysteretic damper

and stiffness of hysteretic dampers for maximizing the damping effect and minimizing the damage to the main frame forms a major design consideration. For structures combined with friction dampers, Paul and Marsh[18] and Filiatrault and Cherry[19] conducted numerical analysis with the slip strength as the variable and found the existence of a slip strength at which the energy dissipated by friction dampers can be maximized. For hysteretic dampers that exhibit elastic–plastic behaviour, Tsai *et al.*[20] and Ciampi *et al.*[21] numerically examined the effect of strength and stiffness of hysteretic dampers on the earthquake response and obtained optimal combinations for the damper's strength and stiffness. These investigations provided important messages for the design of structures combined with hysteretic dampers, but their findings were based only on numerical parametric analysis and therefore remain empirical.

The objective of this paper is to interpret and generalize the optimal condition for the strength and stiffness of hysteretic dampers, by which the damping effect can be maximized. For this purpose, a theoretical relationship that controls the optimal condition is formulated using the concept of the equivalent viscous damping. The hysteretic behaviour of the damping system is assumed to be linear-elastic and perfectly-plastic, and hysteretic behaviour of the main frame is also idealized as linear-elastic and perfectly-plastic. Thus, the hysteretic behaviour of the entire structural system is given as the two linear-elastic and perfectly-plastic models linked in parallel and shown in Figure 4. First, the shear strength of the damper relative to the maximum resistance of the entire structure which maximizes the equivalent viscous damping is derived as a function of relative stiffness of the damper. Then, the validity of the derived shear strength in terms of minimizing the damage to the entire structure is calibrated by numerical analysis for both SDOF and MDOF systems.

OPTIMUM STRENGTH RATIO OF HYSTERETIC DAMPER

The hysteretic behaviour of a structural system with a hysteretic damper is simplified as in Figure 4. The entire system consists of a moment-resisting frame and a hysteretic damper. The relative stiffness k is defined as

$$k = \frac{K_{\mathrm{D}}}{K_{\mathrm{F}}} \tag{1}$$

where K_{D} and K_{F} are the elastic stiffnesses of the damper and main frame, respectively.

The following relations are obtained with reference to Figure 4.

$$\beta Q_{\mathrm{u}} = K_{\mathrm{D}}\Delta_{\mathrm{Dy}},\ (1-\beta)Q_{\mathrm{u}} = K_{\mathrm{F}}\Delta_{\mathrm{Fy}} \tag{2}$$

where β is the ratio of the shear strength of the damper of the strength of the entire structural system, hereafter called the damper's strength ratio. Q_{u} is the ultimate shear strength of the entire structural system, and Δ_{Fy} and Δ_{Dy} are the yield storey drift of the main frame and the damper, respectively.

From the above equations, the following relations can be obtained

$$\frac{\beta}{1-\beta} = \frac{\Delta_{\mathrm{Dy}}}{\Delta_{\mathrm{Fy}}}k = \frac{\mu_{\mathrm{F}}}{\mu_{\mathrm{D}}}k \tag{3}$$

where μ_{F} and μ_{D} are the ductility ratios of the main frame and the damper, respectively.

It is assumed that the damper system should start dissipating the input energy before the main frame yields. This condition is expressed as

$$\mu_{\mathrm{D}} > \mu_{\mathrm{F}} \tag{4}$$

Inequality (4) confines the range of β to:

$$\beta < \frac{k}{k+1} \tag{5}$$

The trigger level (ψQ_{u}) is defined as the strength of the entire system at initial yielding, and the trigger level coefficient (ψ) is expressed as follows:

$$\psi Q_{\mathrm{u}} = \beta Q_{\mathrm{u}} + K_{\mathrm{F}}\Delta_{\mathrm{Dy}} \tag{6}$$

From equations (1), (2) and (6), we obtain

$$\psi = \frac{k+1}{k}\beta \tag{7}$$

Now, we consider the steady-state response of the structural system, as shown in Figure 5. The equivalent viscous damping ratio (h_{eq}) of the hysteretic loop shown in Figure 5 is defined as[22]

$$h_{\mathrm{eq}} = \frac{E_{\mathrm{p}}}{4\pi E_{\mathrm{e}}} \tag{8}$$

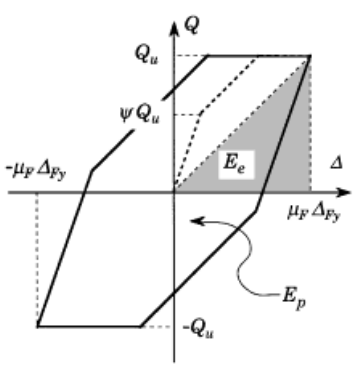

Figure 5. Hysteresis loop of a structure with a hysteretic damper in the steady state

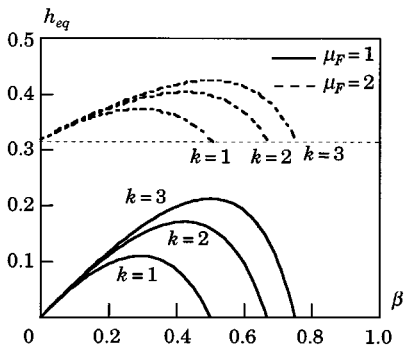

Figure 6. Relationship between equivalent viscous damping ratio (h_{eq}) and damper's strength ratio (β) for various relative stiffness (k) and ductility ratios of the main frame (μ_F)

where E_p is the dissipated energy of the entire system per cycle, and E_e is the area of the hatched triangle in Figure 5. E_p and E_e in equation (8) are expressed, respectively, as follows:

$$E_p = 4[(\mu_D - 1)\Delta_{Dy}\beta + (\mu_F - 1)\Delta_{Fy}(1 - \beta)]Q_u$$

$$E_e = \tfrac{1}{2}\mu_D\Delta_{Dy}Q_u = \tfrac{1}{2}\mu_F\Delta_{Fy}Q_u \tag{9}$$

From equations (3), (8) and (9), the equivalent viscous damping ratio is expressed as

$$\frac{\pi}{2}h_{eq} = 1 - \frac{\beta^2}{(1-\beta)k\mu_F} - \frac{1-\beta}{\mu_F} \tag{10}$$

Figure 6 shows relations between h_{eq} and β for various values of k and μ_F obtained from equation (10) with the constraint given in equation (5). Because E_p in equation (9) increases relative to E_e with increasing k and μ_F, the value of h_{eq} increases with increasing k and μ_F. Figure 6 indicates that h_{eq} takes a peak value in relation to β. The value of β that maximizes h_{eq} is derived as

$$\frac{\partial h_{eq}}{\partial \beta} = 0 \rightarrow \beta_{opt} = 1 - \frac{1}{\sqrt{k+1}} \tag{11}$$

Hereafter, we adopt β_{opt} as the optimum damper's strength ratio because it maximizes the equivalent damping ratio. As is evident from equation (11), β_{opt} depends only on the relative stiffness k and is independent of the ductility ratio of the main frame. This means that the value of β_{opt} is not affected by the degree of damage to the main frame. The corresponding optimum trigger level coefficient (ψ_{opt}) and optimum equivalent damping ratio (h_{opt}) are given by equations (12) and (13), respectively,

$$\psi_{opt} = \frac{k+1}{k}\beta_{opt} = \frac{1}{2-\beta_{opt}} = \frac{1}{k}(k + 1 - \sqrt{k+1}) \tag{12}$$

$$\frac{\pi}{2}h_{opt} = 1 - \frac{2(1-\beta_{opt})}{(2-\beta_{opt})\mu_F} = 1 - \frac{2}{(\sqrt{k+1}+1)\mu_F} \tag{13}$$

The values of β_{opt} and ψ_{opt} are plotted in Figure 7 with respect to the relative stiffness k. Both β_{opt} and ψ_{opt} increase as the value of k increases. It is also notable that the change of ψ_{opt} with k is comparatively small.

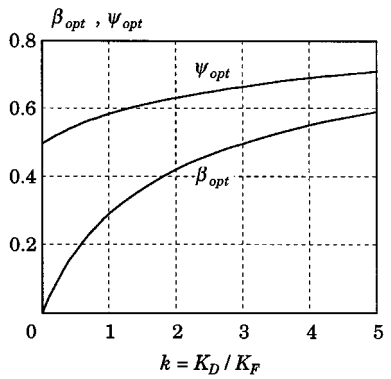

Figure 7. Optimum damper's strength ratio (β_{opt}) and optimum trigger level coefficient (ψ_{opt}) with respect to relative stiffness (k)

EARTHQUAKE RESPONSE OF A SDOF SYSTEM COMBINED WITH A HYSTERETIC DAMPER

Assumptions and method of analysis

Numerical step-by-step time integration was carried out to investigate the effect of the hysteretic damper on the damage to the main frame. The hysteresis model shown in Figure 4 was used for the analysis. The selected variables were: (1) the damper's strength ratio (β), (2) the relative stiffness ($k = 0{\cdot}5, 1{\cdot}0, 2{\cdot}0$), (3) the natural period of the system calculated with respect to the initial elastic stiffness ($K_F + K_D$) and (4) the input earthquake motion. The viscous damping ratio (h) of the system was assumed to be 0·02.

The four ground acceleration records shown in Table I were used, namely the 1940 El Centro earthquake record (N–S component), the 1952 Taft record (E–W component), the 1995 Kobe Meteorological Agency (JMA) record obtained from the Hyogoken–Nanbu Earthquake, and an artificial ground motion designated as 'wv-elns'. The elastic pseudo-velocity spectra (S_V) of these input earthquake motions are shown in Figure 8 for 2 per cent viscous damping.

The ultimate strength of the entire system (Q_u) was determined according to the Japanese seismic code, which is

$$Q_u = C_0 D_S R_t W \tag{14}$$

where C_0 is the base shear coefficient assigned for large earthquakes, D_S is the strength reduction factor determined according to the plastic deformation capacity of the structure, R_t is the normalized design acceleration spectrum, and W is the weight of the structure. According to the Japanese seismic code, the product of C_0 and D_S should not be smaller than 0·25, and 0·30 was selected for $C_0 D_S$. R_t is related to the natural period T of the system as shown in Figure 9.

The earthquake input energy (E_{dm}) that should be absorbed by the entire system is given by the following equation:[13–16]

$$E_{dm} = (E_{Dp} + E_{Fp} + E_e)_{max} \tag{15}$$

where E_{Dp} and E_{Fp} are the hysteretic energies dissipated by the damper and the main frame, respectively, and E_e indicates the elastic vibration energy given as the sum of the strain energy and the kinetic energy. The input energy (E_{dm}) can be expressed in terms of the equivalent velocity (V_{dm}), defined as

$$E_{dm} = \tfrac{1}{2} M V_{dm}^2 \tag{16}$$

where M is the mass of the system.

Table I. Input earthquake motions

Input motion	Max. V. (m/sec)	Max. Acc. (m/sec^2)	Duration (sec)
El Centro NS	0·50	5·11	20
Taft EW	0·50	4·97	20
Kobe NS	0·87	8·18	30
wv-elns	0·54	2·97	30

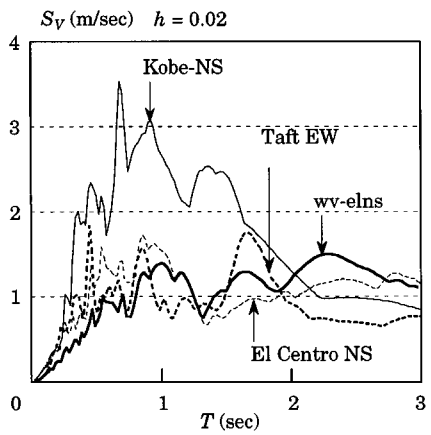

Figure 8. Elastic pseudo-velocity spectra (S_V) of input earthquake motions

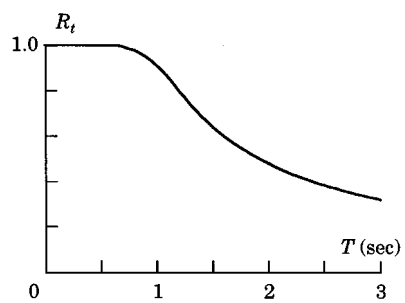

Figure 9. Normalized acceleration spectrum specified by the Japanese seismic design code

The energy dissipated by hysteresis can be converted to another quantity called the ratio of cumulative plastic deformation. This ratio is defined for the hysteretic damper and the main frame as η_D for the damper and η_F for the main frame, thus,

$$\eta_D = \frac{E_{Dp}}{\beta Q_u \Delta_{Dy}}, \quad \eta_F = \frac{E_{Fp}}{(1-\beta) Q_u \Delta_{Fy}} \tag{17}$$

In the above equations, E_{Fp} and η_F represent the damage level of the main frame.

Results of response analysis

Because the response spectrum of the artificial ground motion 'wv-elns' is relatively constant with respect to the natural period and larger in the long period range as compared to other ground motions, the displacement responses for 'wv-elns' were the largest and are therefore emphasized in this section (Figures 10–14). Figure 10 shows the equivalent velocity V_{dm}, of the input energy together with the corresponding elastic pseudo-velocity spectrum (S_V). In this figure, V_{dm} is plotted against various values of β and k. This figure indicates that the input energy to the entire system is relatively independent of the values of β and k, supporting a premise that the energy input during an earthquake is relatively independent of the restoring force characteristics of the structural system.[13–17]

The effect of the damper's strength ratio (β) on the energy dissipated per unit weight by the main frame (E_{Fp}) and the damper (E_{Dp}) are shown in Figures 11 and 12, respectively. The horizontal axis denotes β, and $\beta = 0$ corresponds to the system without a damper. The optimum values β_{opt} obtained from equation (11) are marked by a symbol↓with the superscript indicating the corresponding relative stiffness (k).

Increase of β from zero is accompanied by a rapid decrease of E_{Fp}, indicating a decrease in damage to the main frame. When β exceeds β_{opt}, E_{Fp} increases with β. Thus, damage to the main frame is minimized at β_{opt}. On the other hand, the energy dissipated by the dampers (E_{Dp}) reaches its maximum value near the value of β_{opt}, as shown in Figure 11. This verifies the existence of an optimum value for the damper's strength ratio (β) at which the damper dissipates the most input energy and the damage to the main frame is minimized. Because, as shown in Figure 6, the equivalent viscous damping ratio (h_{eq}) increases for larger k values, the energy dissipated by the damper increases and the energy dissipated by the main frame decreases

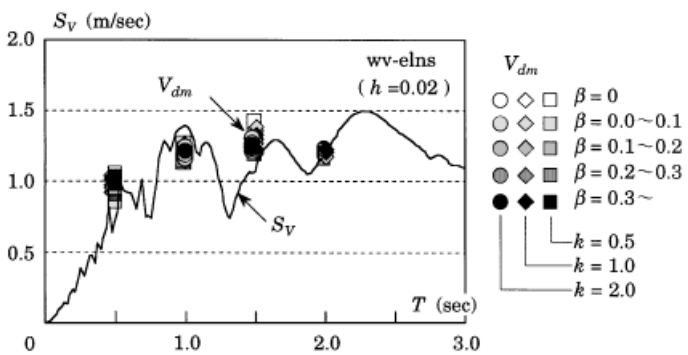

Figure 10. Elastic pseudo-velocity spectrum (S_V) and equivalent velocity of input energy (V_{dm})

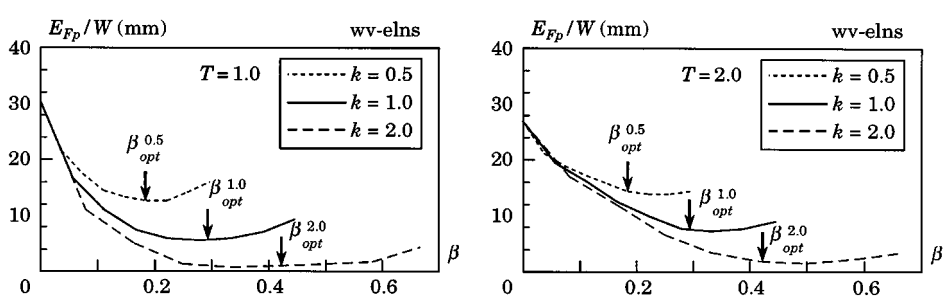

Figure 11. Energy dissipated by the main frame (E_{Fp}) with respect to the damper's strength ratio (β) for various relative stiffnesses (k)

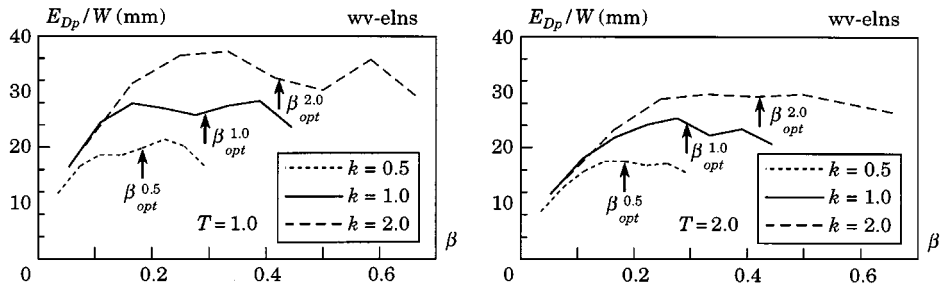

Figure 12. Energy dissipated by the damper (E_{Dp}) with respect to the damper's strength ratio (β) for various relative stiffnesses (k)

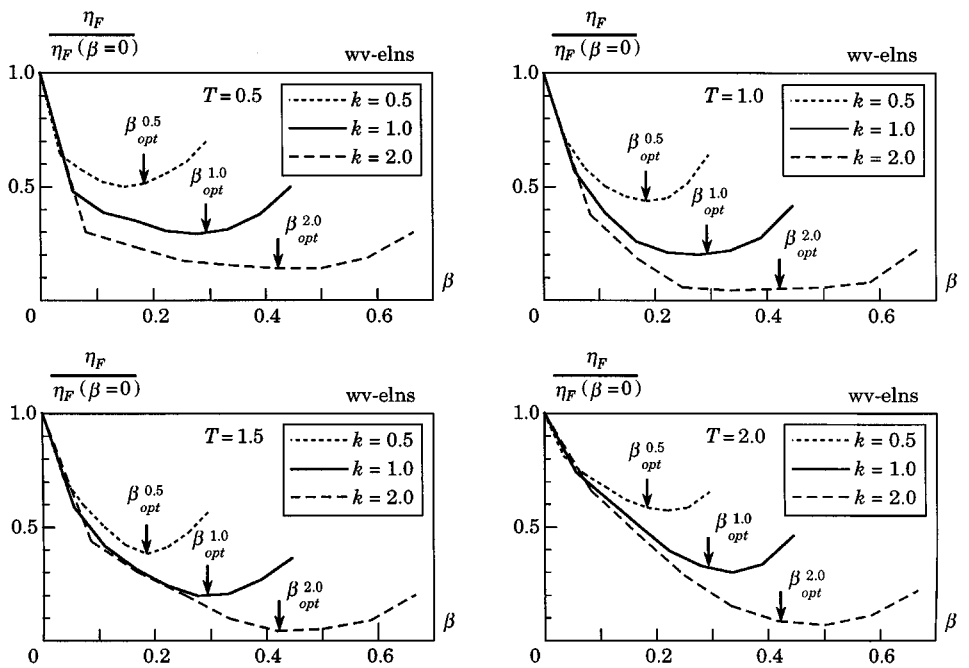

Figure 13. Normalized cumulative plastic deformation of the main frame with respect to the damper's strength ratio (β) for various relative stiffnesses (k)

with the increase of k. Furthermore, with the increase of k, the range in which E_{Fp} reaches its minimum value expands.

Figure 13 shows the effect of β on the damage to the main frame expressed in terms of η_F. The vertical axis is normalized by the η_F obtained for the system without a damper ($\beta = 0$). The behavior shown in Figure 13 is very similar to that obtained for E_{Fp} (Figure 11).

The responses to the four earthquake motions are compared in Figure 14, which shows the relations between η_F and β, as in Figure 13. The value of η_F, an index showing the damage level of the main frame, varies for different earthquake motions. However, the value of β that minimizes η_F is almost the same for all earthquake motions and agrees well with the theoretical value β_{opt} given by equation (11).

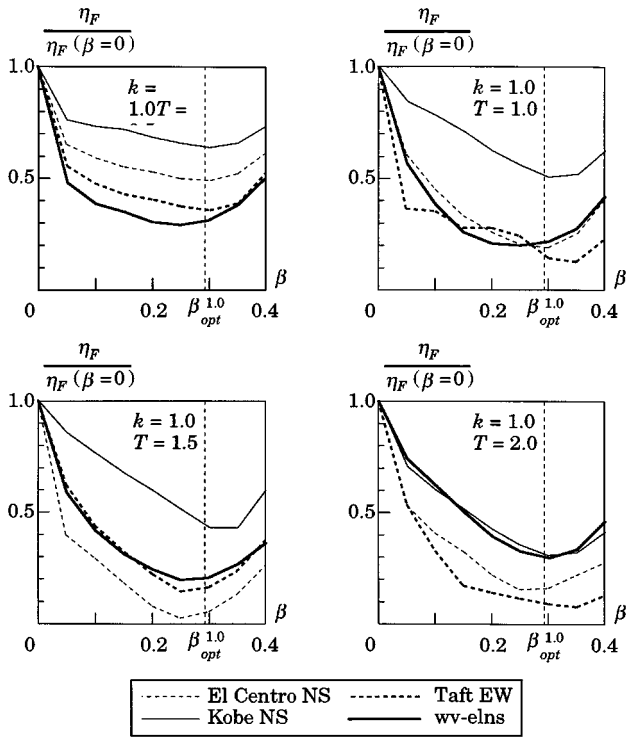

Figure 14. Normalized cumulative plastic deformation of the main frame for various input motions

EARTHQUAKE RESPONSE OF A MDOF SYSTEM COMBINED WITH A HYSTERETIC DAMPER

Assumptions and method of analysis

The results of the earthquake response analysis conducted for a SDOF system confirm: (1) that the energy dissipated by the damper is maximized and the damage to the main frame minimized at a certain β, and that this β is very close to β_{opt} obtained theoretically; and (2) that the range of β in which the energy dissipated by the damper is maximized is rather large, particularly when k is large. To check if these findings are also applicable for multi-storey buildings where hysteretic dampers are arranged in each storey, a series of numerical analysis was carried out for MDOF systems.

Assumptions employed for the analyses were as follows. The mass and the storey height are the same for all storeys, and a height of 4 m is assigned. The hysteresis model of each storey is the same as that used for the analysis of the SDOF system (Figure 4). The damper's strength ratio (β) and the relative stiffness (k) are the same for all storeys. The ultimate strength of the entire system of the ith storey (Q_{ui}) was determined according to the Japanese seismic code, which is

$$Q_{ui} = C_0 D_S R_t A_i W_i \tag{18}$$

where C_0, D_S and R_t are the same as those used in equation (14), W_i is the sum of the weights of storeys above the ith storey, and A_i is the factor that determine the distribution of the storey shear strength along the height of structure. In equation (18), 1·0 was selected for C_0, and 0·25 was selected for D_S. The stiffness of the entire system of the ith storey is determined so that the ith storey drift angle will be 1/200 under the specified static design earthquake force with C_0 set at 0·2. The variables selected in the analysis are: (1) and damper's strength

ratio (β), (2) the relative stiffness ($k = 0{\cdot}5, 1{\cdot}0, 2{\cdot}0$), and (3) input earthquake motion (wv-elns, El Centro NS, Taft EW, Kobe NS). The viscous damping ratio (h) of the system was assumed to be 0·02, and the number of storeys selected for all analyses was 10.

Results of response analysis

The effect of the damper's strength ratio (β) on the total energy dissipated per unit weight by the main frame (E_{Fp}) and the damper (E_{Dp}) are shown in Figure 15(a) and 15(b), respectively. The optimum values β_{opt} obtained from equation (11) are marked by a symbol $\downarrow$ with the superscript indicating the corresponding relative stiffness (k). The figure clearly shows that the energy dissipated by the damper can be maximized and the damage to the main frame minimized around β_{opt}. Figure 16 shows the same relations as in Figure 15 for

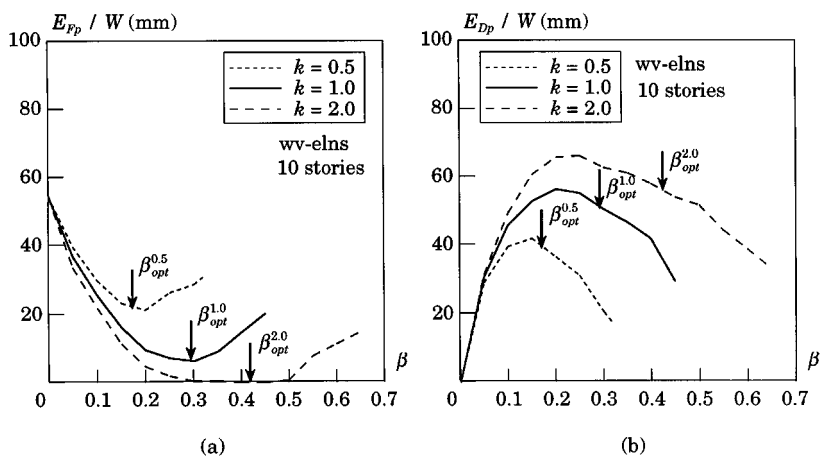

Figure 15. Energy dissipated by main frame (E_{Fp}) and the damper (E_{Dp}) of the 10-storey structure with respect to the damper's strength ratio (β) for various relative stiffnesses (k)

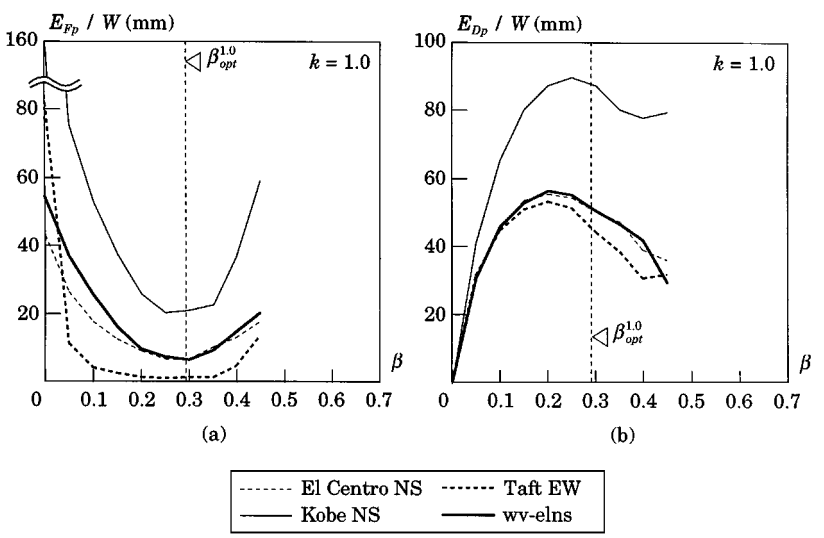

Figure 16. Energy dissipated by the main frame (E_{Fp}) and the damper (E_{Dp}) of the 10-storey structure with respect to the damper's strength ratio (β) for various input motions

the four ground motions. The values of β that minimize the energy dissipated by the main frame (E_{Fp}) are almost the same for all ground motions and correspond satisfactorily with the theoretical optimum values for β_{opt}.

CONCLUSION

This study of the effect of hysteretic dampers on the damage to main frames when subjected to severe earthquakes is summarized as follows:

(1) The optimum damper's strength ratio (β_{opt}) that maximizes the equivalent viscous damping ratio was derived theoretically. It was found that β_{opt} depends only the relative stiffness (k) and is independent of the level of plastic deformation of the main frame
(2) The results of numerical response analyses for both SDOF and MDOF systems confirm that the energy dissipated by dampers can be maximized and the damage to the main frame minimized at a certain β, and that this β is very close to the β_{opt} obtained theoretically.
(3) The range of β in which the energy dissipated by dampers is maximized is rather large, i.e. one has even with some deviation of β from β_{opt} the benefit of the dampers.
(4) The values of β that minimize the damage to the main frame remain relatively unchanged regardless of the type of ground motion and correspond satisfactorily with the theoretical optimum values.

REFERENCES

1. R. D. Hanson *et al*., 'State-of-the-art and state-of-the-practice in seismic energy dissipation', *Proc. Seminar on Seismic Isolation, Passive Energy Dissipation, and Active Control*, Vol. 2, Applied Technology Council, 1993, pp. 449–471.
2. R. D. Hanson, 'Supplemental damping for improved seismic performance', *Earthquake Spectra EERI* **9**, 319–334 (1993).
3. I. D. Aiken *et al*., 'Testing of passive energy dissipation systems', *Earthquake Spectra EERI* **9**, 335–370 (1993).
4. S. F. Stiemer, W. G. Godden and J. M. Kelly, 'Experimental behavior of a spatial piping system with steel energy absorbers subjected to a simulated differential sseismic input', *Report No. UCB/EERC-81/109*, Earthquake Engineering Research Center, 1981.
5. A. Whittaker, V. V. Bertero and J. Alonso, 'Earthquake simulator testing of steel plate added damping and stiffness elements', *Report No. UCB/EERC- 89/102*, Earthquake Engineering Research Center, University of California, Berkeley, CA, 1989.
6. K. C. Tsai and C. P. Hong, 'Steel triangular plate energy absorber for earthquake resistant buildings', *Proc. 1st World Conf. on Constructional Steel Design*, Acupulco, 1992, pp. 345–355.
7. Y. Shinabe and Y. Takahashi, 'The present state of eccentric brace design in Japan', *Structural Steel, 4th Pacific Structural Steel Conf*., Vol. 1, 1995.
8. M. Nakashima *et al*., 'Energy dissipation behavior of shear panels made of low yield steel', *Earthquake Engng. Struct. Dyn.* **23**, 1299–1313 (1994).
9. S. Cherry and A. Filiatraut, 'Seismic response control of buildings using friction damper', *Earthquake Spectra EERI* **9**, 447–466 (1993).
10. C. E. Grigorian, T. S. Yang and E. P. Popov, 'Slotted bolted connection energy dissipation', *Earthquake Spectra EERI* **9**, 491–504 (1993).
11. S. Ono, K. Nakahira, S. Tsujioka and K. Inoue, 'Static and dynamic hysteresis characteristics of thermally sprayed aluminium friction damper', *J. Struct. Engng. AIJ* **41B**, 1–8 (1995) (in Japanese).
12. K. Inoue, Y. Higashibata and K. Inoue, 'Lateral bracing criteria of the composite braces', *Proc. ASCE Structures Congr. XII*, ASCE, Vol. 1, 1994, pp. 152–157.
13. G. W. Housner, 'Limit design of structures to resist earthquake', *Proc. 1st WCEE*, Berkeley, California, 1956, pp. 5.1–5.13.
14. G. W. Housner, 'Behavior of structures during earthquake', *J. Engng. Mech. ASCE* **4**, 109–129 (1959).
15. T. F. Zahrah and W. J. Hall, 'Earthquake energy absorption in SDOF structure', *J. Struct. Engng. ASCE* **110**, 1757–1772 (1984).
16. H. Akiyama, *Earthquake-resistant Limit-state Design of Buildings*, University of Tokyo Press, Tokyo, Japan, 1985.
17. M. Nakashima, K. Saburi and B. Tsuji, 'Energy input and dissipation behaviour of structures with hysteretic dampers', *Earthquake Engng. Struct. Dyn.* **25**, 483–496 (1996).
18. A. S. Pall and C. Marsh, 'Response of friction damped braced frames', *J. Struct. Div. ASCE* **108**, 1313–1323 (1982).
19. A. Filiatrault and S. Cherry, 'Seismic design spectra for friction-damped structure', *J. Struct. Engng. ASCE* **116**, 1334–1355 (1990).
20. K. C. Tsai, W. H. Chen, C. P. Hong and Y. F. Su, 'Design of steel triangular plate energy absorbers for seismic-resistant construction', *Earthquake Spectra EERI* **9**, 505–528 (1993).
21. V. Ciampi, M. D. Angelis and F. Paolacci, 'Design of yielding or friction-based dissipative bracings for seismic protection of buildings', Engng. Struct. **17**, 381–391 (1995).
22. L. S. Jacobsen, 'Damping in composite structures', *Proc. 2nd WCEE*, Tokyo, 1960, pp. 1029–1044.

